Lab on a Chip

View Online
Dynamic Article Links

Cite this: *Lab Chip*, 2011, **11**, 93

www.rsc.org/loc

**PAPER**

# Multistage-multiorifice flow fractionation (MS-MOFF): continuous size-based separation of microspheres using multiple series of contraction/expansion microchannels†

**Tae Seok Sim,‡[a] Kiho Kwon,‡[b] Jae Chan Park,[a] Jeong-Gun Lee*[a] and Hyo-Il Jung*[b]**

***Received 15th June 2010, Accepted 26th August 2010***
**DOI: 10.1039/c0lc00109k**



Previously we introduced a novel hydrodynamic method using a multi-orifice microchannel for size-based particle separation, which is called a multi-orifice flow fractionation (MOFF). The MOFF has several advantages such as continuous, non-intrusive, and minimal power consumption. However, it has a limitation that the recovery yield is relatively low. Although the recovery may be increased by adjusting parameters such as the Reynolds number and central collecting region, poor purity inevitably followed. We newly designed and fabricated a microfluidic channel for multi-stage multi-orifice flow fractionation (MS-MOFF), which is made by combining three multi-orifice segments, and consists of 3 inlets, 3 filters, 3 multi-orifice segments and 5 outlets. The structure and dimensions of the MS-MOFF were determined by the hydrodynamic principles to have constant Reynolds numbers at each multi-orifice segment. Polystyrene microspheres of two different sizes (7 μm and 15 μm) were tested. With this device, we made an attempt to improve recovery and minimize loss of purity by collecting and re-separating non-selected particles of the first separation. The final recovery successfully increased from 73.2% to 88.7% while the final purity slightly decreased from 91.4% to 89.1% (for 15 μm). These values were never achievable with the single-stage MOFF (SS-MOFF) having only one multi-orifice segment in our previous work. The MS-MOFF channel will be useful for clinical applications, such as separation of circulating tumor cells (CTC) or rare cells from human blood samples.

## 1. Introduction

Separation technology using microfluidic devices has emerged as an efficient technology that allows the user to purify microparticles, such as polymer beads, biological cells, emulsions, and colloids from a variety of biological and environmental samples, which can then be isolated and collected for downstream testing. Numerous techniques have been developed to achieve this purpose and in general can be divided into two categories, active and passive. In the case of active separation methods, which include electrophoresis,[1,2] dielectrophoresis,[3–6] magnetophoresis,[7–9] ultrasound,[10,11] centrifugation,[12] gravitation,[13,14] and optical manipulation,[15–17] an external energy source is normally required to manipulate the migration of particles in the microfluidic environment. Although these active methods provide good separation accuracy, they are normally limited to low throughput and require a precision instrument for the additional energy source.

Passive separation methods induce changes in particle behavior using hydrodynamic effects that are driven by the geometrical features of microchannels. Passive methods have received significant attention in the past decade owing to the discoveries of many interesting fluid dynamic phenomena in microfluidics. These discoveries provided many opportunities to researchers to develop the hydrodynamic separation methods, such as particle size-based lateral displacement or filtration performed using a patterned array of micropillars,[18] a particle-pinched effect with a sheath flow,[19,20] and a splitting flow to a side channel.[21–23] Such approaches have an advantage that preserves sample condition since they do not require labeling processes that are essential to several active methods. However, they require a laminar flow associated with low Reynolds numbers, which has the effect of prolonging operation time. New approaches in hydrodynamic separation using secondary flow in a microfluidic channel have recently been introduced. In these methods, lateral particle migration is induced by secondary flow generated on a cross section by specific geometric properties of microchannels: for example, lateral flow by three-dimensional

[a]*Bio Lab, Emerging Tech. R&D Center, Samsung Advanced Institute of Technology, San 14, Nongseo-dong, Giheung-gun, Younin-si, Gyeonggi-do, 446-712, Republic of Korea. E-mail: biogun.lee@samsung.com; Fax: +82-13-280-8277; Tel: +82-31-280-6989*
[b]*School of Mechanical Engineering, Yonsei University, 262 Seongsan-no Seodaemun-gu, Seoul, 120-749, Republic of Korea. E-mail: uridle7@yonsei.ac.kr; Fax: +82-(0)2-312-2159; Tel: +82-(0)2-2123-5814*
† Published as part of a LOC themed issue dedicated to Korean Research: Guest Editors: Professor Je-Kyun Park and Kahp-Yang Suh
‡ These authors contributed equally to the work.

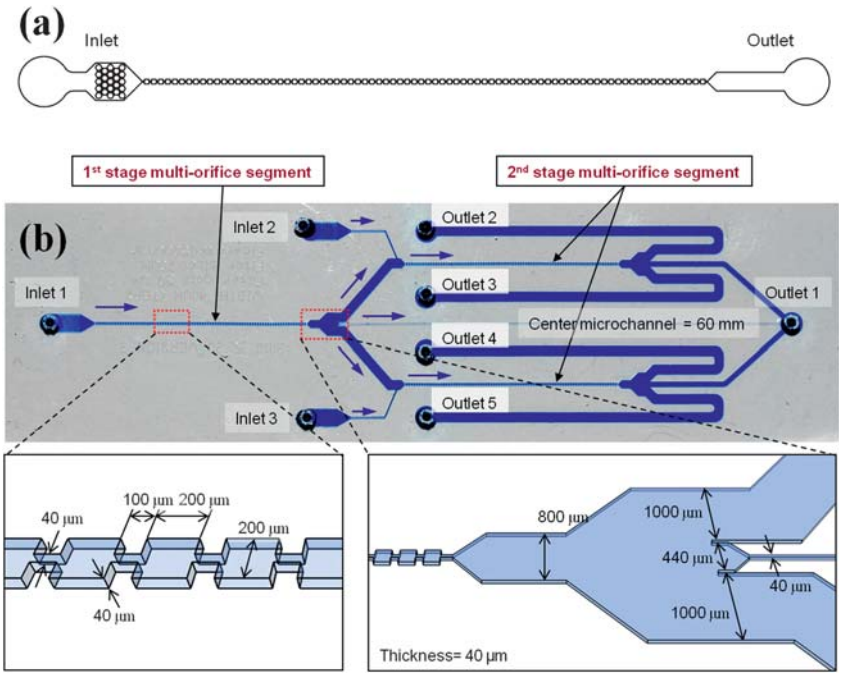


**Fig. 1** Comparative schematic view of two kinds of multi-orifice flow fractionation (a) the single-stage multi-orifice flow fractionation (SS-MOFF), (b) the multi-stage multi-orifice flow fractionation (MS-MOFF).

(3-D) slanted obstacles[24,25] and Dean flow in curved rectangular channels.[26–28] These methods attain lateral particle displacement with differential inertial effects according to particle size.[29] With these techniques, biological and polymer particles could be separated in a continuous flow with a moderate flow rate and a low particle concentration. Also, another passive-type separation method was recently introduced on the basis of a trajectory mismatch between particle and fluid by momentum loss, which was controlled by asymmetric sheath flows.[30]

In a previous study, we introduced a novel hydrodynamic method for particle focusing using a multi-orifice microchannel[31] and subsequently demonstrated the feasibility of our hydrodynamic method for size-based particle separation.[32] Our new separation method was named multi-orifice flow fractionation (MOFF), since the microparticle was moved laterally by hydrodynamic inertial forces driven by a multi-orifice structure (Fig. 1a). The extent of lateral movement varies according to particle size, and polymer microspheres can be concentrated separately at different lateral positions in a microchannel. The separation efficiency is mostly affected by the Reynolds number (*Re*) and the central collecting region in the channel. By adjusting the width and position of a central collecting region in the outlet, the separation efficiency could be optimized. However, since the recovery has a reciprocal relationship with the purity, there are still limitations to increase both recovery and purity. In this work, we propose a multi-stage multi-orifice flow fractionation (MS-MOFF) method to improve recovery and minimize loss of purity.

## 2. Materials and methods

### 2.1. Design and fabrication of the device

The single-stage multi-orifice flow fractionation (SS-MOFF) consists of an inlet, a filter, a multi-orifice segment, and an outlet (Fig. 1a). The multi-orifice segment is an alternating series of contraction and expansion channels, through which particles are separated by the momentum-change-induced inertial force. The widths of the contraction and expansion channels are 40 μm and 200 μm, respectively. Each expansion region is 200 μm in length and linked with 100 μm contraction channel. This series of orifice patterns is repeated 80 times and has 40 μm thicknesses. Fig. 1b shows the fabricated device and schematic configurations of the multi-stage multi-orifice flow fractionation (MS-MOFF). The MS-MOFF is formed by combining 3 multi-orifice segments and consists of 3 inlets, 3 filters, 3 multi-orifice segments and 5 outlets. The dimensions of the multi-orifice segment in the first stage are the same as those of the SS-MOFF. In the second stage, the central channel is 40 μm wide and 60 mm long. Each branched side channel has 1 mm width and 10 mm length, and connects with the second stage MOFF. A particle mixture (7 μm and 15 μm microspheres) is injected from inlet 1 using a syringe pump, and then the target particles, in our case 15 μm particles, are focused on the centerline of the multi-orifice segments in the first stage and directly transported to the outlet *via* the center microchannel in the second stage. The mixture including the remaining target particles (remnant of 15 μm particles and most of the 7 μm particles) flows through the side microchannels. Buffers are added from inlet 2 and 3 to compensate the flow rate through the multi-orifice segments in the second stage. The separated target particles are collected to outlet 1, and other particles are collected to outlet 2–5.

The MS-MOFF device was fabricated by soft-lithography techniques. We used 6 inch silicon wafer as substrate, and SU-8 (SU-8 2050, MicroChem., Massachusetts) was used for channel master mold. Finally, the MS-MOFF device was replicated with PDMS (Sylgard 184, Dow Corning Corp., Michigan). The 10 : 1 volumetric mixture of PDMS and a curing agent was poured on

 

the master mold. After degassing the PDMS mixture, the wafer was placed on a hot plate at 75 °C for 60 min. And then, the cured polymer mixture was taken off from the master mold. The MS-MOFF patterned polymer was punched at inlet and outlet and bonded to clean glass after plasma treatment (plasma generator, Cute-B Plasma, FEMTO Science, Korea).

### 2.2 Preparation of particle suspension

Fluorescent polystyrene microspheres 7 μm (35-2, green, 468/508 nm) and 15 μm (36-4, red, 542/612 nm) in diameter were used for the particle suspensions (Thermo Fisher Scientific Inc., Massachusetts). The specific gravity of the two kinds of microsphere was about 1.05, and the microspheres were prepared in a 0.5 wt % Tween 20 (Sigma-Aldrich Co., Missouri) aqueous solution. Initial particle concentrations of 15 μm and 7 μm particles is $7.7 \times 10^3$/μL and $10.1 \times 10^3$/μL, respectively. After measuring the flow of the individual particles, the two kinds of particles were mixed and applied to the simultaneous flow measurement.

### 2.3 Operation

We used a syringe pump (KDS200, KD Scientific, Massachusetts) to generate a continuous and stable micro flow. The 1 mL syringe was connected to inlet 1 for sample, and a 10 mL syringe was connected to inlet 2 and 3 for compensation buffer. The flow rate of inlet 1 was 102 μL $min^{-1}$, and the flow rate of inlet 2 and 3 was 61.2 μL $min^{-1}$. Each flow rate was determined by the Reynolds number of the multi-orifice segments ($Re = 85$). Prior to each experiment, we performed a degassing process by filling with 70% ethanol and then pushing away ethanol with DI water. This was done since low polarity solvent more easily wets the hydrophobic PDMS surface. An inverted optical microscope (I-70, Olympus, Japan) was used to observe the behavior of fluorescent particles beyond the glass part of the microchannel. The microscope was equipped with a 100 W mercury lamp and fluorescence mirror unit (U-MWB2, U-MWG2, U-MWU2; Olympus, Japan) for obtaining color images of the two (red, green) fluorescent particles. A color CCD camera (ProgRes C10, JENOPTIK, Germany) was used to take the fluorescent images, which were post-processed with imageJ (NIH, Maryland) and Matlab (The MathWorks, Massachusetts).

## 3 Results and discussion

The Reynolds number ($Re$) of the microchannel can be varied by the dimension of the microchannel and flow rate. Since the multi-orifice segment in the first stage and two multi-orifice segments in the second stage have the same dimensions, the $Re$ of the two multi-orifices in the second stage is only controlled by the flow rates. The multi-orifice segment in the end of the first stage is divided by a center microchannel and two side channels (Fig. 1b). The division leads to the variation of the flow rate in the second stage compared with that in the first stage, which alters the $Re$. To maintain the $Re$ consistent from the first to the second stage, buffer solution was injected into inlet 2 and 3 at the same time. It is important to define the fluidic resistances in the second stage microchannels. When the fluidic resistances in the second stage microchannels are not well defined, fluids from the inlets in the second stage might hinder or change the direction of fluid from the first stage. In particular, if the center microchannel for collecting the target particle has near zero fluidic resistance, most of the fluids from the first stage would flow through the center microchannel in the second stage. Therefore, based on the well-known analogy between fluidic circuits and electrical circuits, the fluid flowing through the microchannel network was expressed by the equivalent electrical circuit. Inlets for the fluid injection and microchannels of the MS-MOFF serve as the current sources and resistances, respectively. Fig. 2 shows the equivalent electrical circuit of the MS-MOFF. As maximum purity was obtained at 140 μm width of central collecting region (18% of the outlet width) in our previous work,[32] the flow rate through the center microchannel ($Q_{Rc}$) would be 18% flow rate of the multi-orifice segment ($Q_{RI}$) of the first stage. From the given flow rate, $Qs$ can be calculated by Kirchhoff's law as follows,

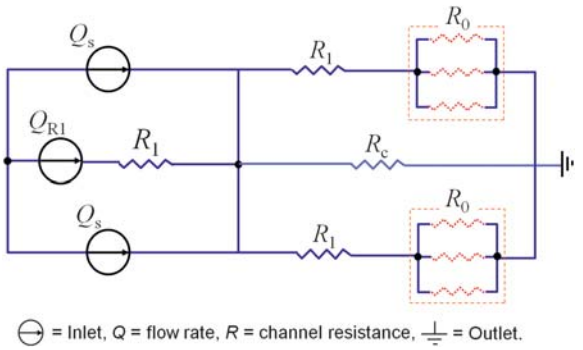


**Fig. 2** The equivalent electrical circuit of the multi-stage multi-orifice flow fractionation channel.

$$2\,Q_{R1} + Q_{Rc} = 2\,Q_s + Q_{RI} \quad (1)$$

Here, the $Q_{RI}$, $Q_s$, and $Q_{Rc}$ are the flow rates through the multi-orifice segment, the inlet of the second stage and the center microchannel, respectively.

Then, the relationship of $Q_s$ and $Q_{RI}$ can be defined as

$$Q_s = 0.59\,Q_{RI} \quad (2)$$

Since the outlets of the second stage are designed to have relatively large width compared with that of the multi-orifice segment and the center microchannel, we may assume $R_0 \ll R_1$.

Then, $R_c$ can be calculated by the following equation,

$$R_c Q_{Rc} = R_1 Q_{R1} \quad (3)$$

Here, $R_1$, $R_c$, $R_0$ are the fluidic resistances of the multi-orifice segment, the center microchannel and the outlet, respectively.

From the above equation, the relationship between $R_c$ and $R_1$ is given by

$$R_c = \frac{R_1}{0.18} \quad (4)$$

Therefore, if the dimensions of the multi-orifice segment are given, the dimensions of the center microchannel could be

acquired by calculating the fluidic resistances. The fluidic resistance of an arbitrary rectangular channel is defined by

$$R = \frac{f\mathrm{Re}}{2}\frac{\mu l}{D_h^2 A} \quad (5)$$

Where $f$Re is the laminar friction constant, $\mu$ is the dynamic viscosity (N s m$^{-2}$), $l$ is the channel length (m), $D_h$ is the hydraulic diameter (m), and $A$ is the channel cross sectional area of the channel (m$^2$). The laminar friction constants may be determined analytically for various aspect ratio ($\alpha$) as follows. The aspect ratio is defined as either height/width or width/height such that $0 < \alpha < 1$.[33]

$$f\mathrm{Re} = 96(1 - 1.3553\alpha + 1.9467\alpha^2 - 1.7012\alpha^3 + 0.9564\alpha^4 - 0.2537\alpha^5) \quad (6)$$

Next, the hydraulic diameter is given by

$$D_h = \frac{2ab}{(a+b)} \quad (7)$$

Where $a$ and $b$ are the width and the height of the arbitrary rectangular channel.

Since we have already discussed the effects of the *Re* and the central collecting region on the separation efficiency in our previous work,[31,32] it is not necessary for the purpose of this work to enter into a detailed description of the optimization procedures for the MS-MOFF. According to our previous results with regards to the SS-MOFF, the size based particle separation could be best achieved in the specific range of the *Re* of 63–91. Various *Re* within the range of 63–91 were tested to obtain the best separation yields, and *Re* of 85 was selected for our experiments. Particle trajectories were acquired by a fluorescence microscope with 50× magnification. First, the feasibility of the MS-MOFF was verified by visualization. Using the acquired fluorescence images, fluorescence intensity was subsequently exploited to analyze quantitative particle distribution, which indirectly represents particle population. Image data was converted to numerical data using Matlab. The converted intensity data were gathered along a detection line that was located at 1 mm position of the broadened outlet channel away from the final contraction channel. In the imaging analysis, accuracy of the intensity level could be influenced by a few factors, such as particle retention time in the field of view, particle concentration, depth of focus, and channel depth. First, we reduced exposure time of the CCD camera to prevent overlapping of particle streaks due to a long retention time. Finally, the microscopy system acquired fluorescence images with the depth of focus approximately 10 μm smaller than the channel depth (50 μm). With the converted numerical intensity, we calculated recovery and purity. Recovery was defined as partial fraction of separating particles relative to total injected particles, and purity of each particle was defined as cross-contamination of different sizes of the particles.

Fig. 3 shows progress of particle migration through the multi-orifice segments in the second stage. The measurement positions in the upstream, the midstream, and the downstream corresponded to the first, the 40th, and the 80th orifices, respectively. Inertial lift force inducing particle migration began to affect the particle distribution after around the 35∼45th orifice, and the stable particle distribution was observed at around the 70∼80th orifice. Although the 7 μm particles clustered near to both side walls in the first stage, they gathered at only one side of the wall in the second stage. This phenomenon can be explained by the reason that the 7 μm particles tend to only flow near to the side wall at $Re = 85$. When the 7 μm particles are biased to one side due to the buffer flows from inlet 2 and 3, they never exceed the centerline of multi-orifice segment. Thus the biased particles keep biased to the same side until the end of multi-orifice segment. On the other hand, the 15 μm particles are not biased rather are focused to the centerline of the multi-orifice segment caused by the momentum change induced inertial force repelling from the side wall at $Re = 85$. Fig. 4 clearly exhibits the independently experimented particle distributions for the 7 μm and

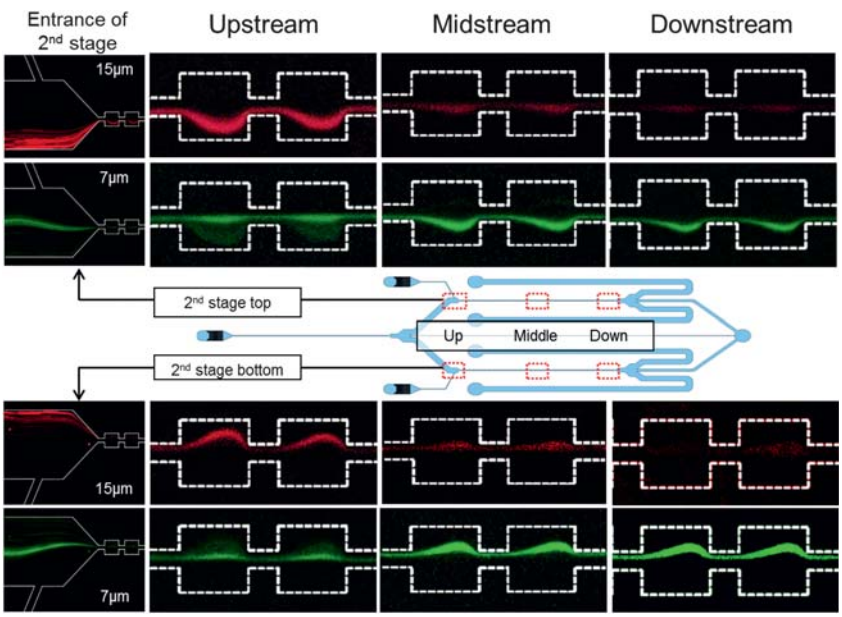


**Fig. 3** Photographs of the particle migration progress through the second stage multi-orifice segments (top and bottom) at $Re = 85$.

 

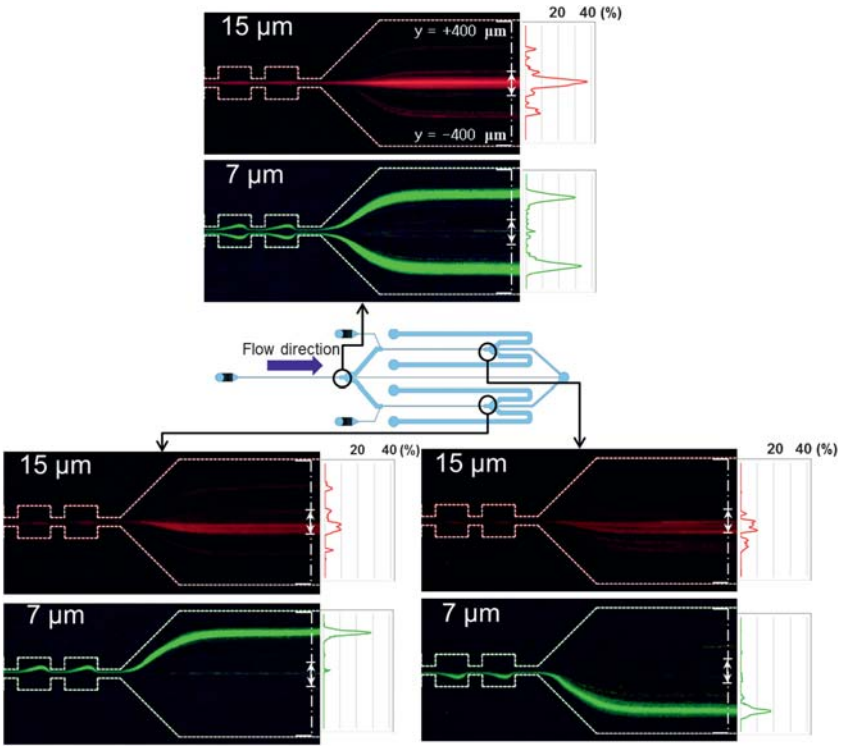


**Fig. 4** Photographs of the particle trajectories and the fluorescence distribution curves in the end of each MOFF segment from independent experiment of the two (15 and 7 μm) polystyrene microspheres at $Re = 85$. (The alternated long and short dash lines indicate detection lines).

15 μm polystyrene microspheres after passing downstream of the multi-orifice segments. The relative intensity distribution curves of each polystyrene microsphere at the detection line are also shown beside each fluorescent image. In the case of the 15 μm particles, most particles passed through the centerline of the microchannel at the range of $y = -70$ μm to $y = 70$ μm (140 μm out of the 800 μm broaden outlet width). On the other hand, the 7 μm particles tended to pass through near the sidewall (at $y < -70$ μm or $y > 70$ μm). It was also shown that the fluorescence intensity of the particle distribution reduced in the second stage because the separated particles in the first stage were divided at the channel division area and diluted by buffer solution from inlet 2 and 3. In particular, the 15 μm particles were almost separated in the first stage and half of the remaining particles divided into top and bottom multi-orifice segments in the second stage, and buffer solution from the inlet 2 and 3 further diluted the particles. Therefore, the fluorescence intensity of the 15 μm particles decreased more than that of the 7 μm particles. The reduced intensity of the 15 μm particles in the second stage was 23% of the intensity in the first stage. On the contrary, the intensity of the 7 μm

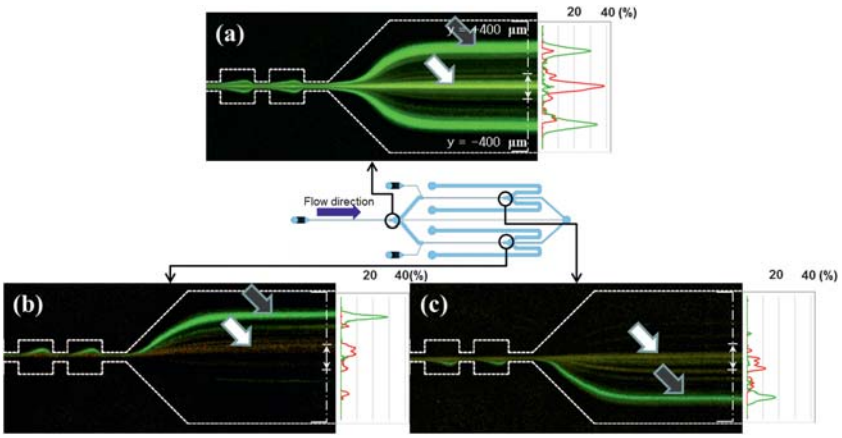


**Fig. 5** 3 Photographs of simultaneous experiments using a mixture of the two polystyrene microspheres at $Re = 85$. Schematic view of MS-MOFF and position of image captured. (a) End of the 1st multi-orifice segment. (b) End of the 2nd top multi-orifice segment. (c) End of the 2nd bottom multi-orifice segment (dark arrows indicate the 7 μm particles and white arrows indicate the 15 μm particles, respectively). (The alternated long and short dash lines indicate detection lines).

**Table 1** Separation efficiency comparison of MS-MOFF and SS-MOFF[a]

| | | | SS-MOFF[32] | | MS-MOFF | | | | |
|---|---|---|---|---|---|---|---|---|---|
| | | Particle diameter | $Re_c = 70$ | $Re_c = 98$ | 1st stage | | 2nd top | 2nd bottom | Total |
| Recovery | Center | 15 μm | 65.0 | 75.2 | 73.2 | | 52.6 | 61.1 | 88.7 |
| | | 7 μm | 1.4 | 15.6 | 4.01 | | 4.2 | 3.5 | 7.6 |
| | Side | 15 μm | 11.1 | 8.9 | 10.6[b] | 16.2[c] | 47.4 | 38.9 | 11.3 |
| | | 7 μm | 93.7 | 49.5 | 41.8[b] | 54.1[c] | 95.8 | 96.5 | 92.4 |
| Purity | Center | 15 μm | 90.8 | 49.6 | 91.4 | | 90.2 | 94.4 | 89.1 |
| | | 7 μm | 9.2 | 50.4 | 8.6 | | 9.8 | 5.9 | 10.9 |
| | Side | 15 μm | 2.2 | 3.4 | 12.8 | | 26.6 | 27.7 | 7.9 |
| | | 7 μm | 97.8 | 96.6 | 87.2 | | 73.4 | 72.3 | 92.1 |

[a] The values with superscript indicate each side of recovery. (b: side top channel, c: side bottom channel).



particles only reduced to an average of 72% of the intensity in the first stage. Fig. 5 shows photographic images of separation results using a mixture of two different sizes of the polystyrene microspheres (7 μm and 15 μm) in the MS-MOFF at $Re = 85$. The relative intensity curves for each fluorescent image are also depicted in Fig. 5. Trajectory of the 15 μm particles is shown as yellow (white arrow) whereas trajectory of the 7 μm particles is shown as green (dark arrow). Since the fluorescent images were acquired by the green fluorescent filter cube (U-MWB2, Olympus). The red color looks like yellow color when presenting two colors (red and green) at the same time. The images and the intensity graphs demonstrated that the distribution of the two particles is quite well districted. The particles behaved differently and independently with respect to the particle size. The particle distribution of a particle mixture was similar to that of individual particles shown in Fig. 4. And the intensity differences between individual and mixture samples were within 2.6%, which is indicating that our MS-MOFF can separate two different sizes of beads from a mixture. Table 1 summarizes the recovery and the purity of two-sized particles that were concentrated at the central collecting region (140 μm out of 800 μm outlet width) and side sections according to three multi-orifice segments. The recovery of the 15 μm particles could be achieved up to 90.1% by increasing the width of the central collecting region to 300 μm (38% of the 800 μm outlet width) and the *Re* to 90, respectively in our previous work. However, experimental results revealed that the purity significantly decreased along with the increase of the central collecting region width. The enlarged central collecting region was responsible for the poor purity. The acquired purity was only 30.4%. Therefore, we decided not to consider the 300 μm width in this work. The maximum purity (90.8%) was obtained at 140 μm width of the central collecting region (18% of the outlet width) and $Re = 70$, but the recovery was only 65%. Although we tried to increase the recovery by increasing the *Re* from this maximum purity condition, it was revealed that the purity of the 15 μm particles dramatically decreased along with the increase in recovery when the width of the central collecting region was 140 μm. The recovery only increased from 65% to 75.2% while the purity significantly decreased from 90.8% to 49.6%. We compared these results with that of the MS-MOFF in Table 1, as suggested in the design consideration; recovery through the MS-MOFF was improved with minimized loss of purity. The final recovery increased from 73.2% to 88.7% while the final purity slightly decreased from 91.4% to 89.1%. These values were never achievable with the SS-MOFF in our previous work. Since the recovery has a reciprocal proportion with the purity when adjusting the *Re* or the width of the central collecting region, it was theoretically impossible to improve both recovery and purity at the same time using the SS-MOFF. The recovery differences between the first and the second stage result from the inconsistent *Re* of each multi-orifice segment due to unknown factors affecting flow conditions, which is beyond the topic of this work. More experiments are needed to find these unknown factors in the future.

## 4. Conclusions

We described a new method for improving recovery and minimizing loss of purity in particle separation using several multi-orifice flow fractionations (MOFF). The newly designed and fabricated microfluidic channel for multistage multi-orifice flow fractionation (MS-MOFF) is constructed by combining three multi-orifice segments and consists of 3 inlets, 3 filters, 3 multi-orifice segments and 5 outlets. Structure and dimensions of the MS-MOFF were determined by the hydrodynamic principles to have consistent Reynolds numbers at each multi-orifice segment. With this device, we made an attempt to improve recovery and minimize loss of purity by collecting and re-separating non-selected particles of the first separation. This method was demonstrated through confirmation of separation performance using microspheres of two different sizes (7 μm and 15 μm). As expected, we could improve recovery of 15 μm particles with the minimized loss of purity. The final recovery successfully increased from 73.2% to 88.7% while the final purity slightly decreased from 91.4% to 89.1% at $Re = 85$, which were never achievable with the single-stage MOFF (SS-MOFF) in our previous work. Separation throughput of the MS-MOFF was approximately 1–5 $\times$ $10^4$ particles/s. According to our experimental results, the MS-MOFF composed of more than three stages would give rise to nearly 100% recovery and 90% purity. In future work, the MS-MOFF will be developed further for clinical applications, such as separation of circulating tumor cells (CTC) or rare cells from human blood samples, which need high recovery near to 100%.

## Acknowledgements

This research was supported by Research Programs (Grant No. 2009-0072750, 2008-05943) through the National Research Foundation of Korea (NRF) funded by the Ministry of

 

Education, Science and Technology. Research facilities are kindly provided by the National Core Research Center (NCRC) for Nanomedical Technology (Grant No. R15-2004-024-00000-0) of the National Research Foundation and by a Grant from the ICBIN of the Seoul R&BD program (Grant No. 10816). We thank Dr Minseok Kim and Eunchul Cho for helpful discussion and technical assistance.

## References

1 S. P. Radko and A. Chrambach, *Electrophoresis*, 2002, **23**, 1957–1972.
2 K. D. Caldwell and Y. S. Gao, *Anal. Chem.*, 1993, **65**, 1764–1772.
3 X. B. Wang, J. Yang, Y. Huang, J. Vykoukal, F. F. Becker and P. R. C. Gascoyne, *Anal. Chem.*, 2000, **72**, 832–839.
4 R. Pethig, *Crit. Rev. Biotechnol.*, 1996, **16**, 331–348.
5 H. Morgan, M. P. Hughes and N. G. Green, *Biophys. J.*, 1999, **77**, 516–525.
6 P. R. C. Gascoyne and J. Vykoukal, *Electrophoresis*, 2002, **23**, 1973–1983.
7 H. Watarai, M. Suwa and Y. Iiguni, *Anal. Bioanal. Chem.*, 2004, **378**, 1693–1699.
8 N. Pamme and C. Wilhelm, *Lab Chip*, 2006, **6**, 974–980.
9 C. H. Ahn, M. G. Allen, W. Trimmer, Y. N. Jun and S. Erramilli, *J. Microelectromech. Syst.*, 1996, **5**, 151–158.
10 F. Petersson, L. Aberg, A.-M. Sward-Nilsson and T. Laurell, *Anal. Chem.*, 2007, **79**, 5117–5123.
11 J. J. Hawkes and W. T. Coakley, *Sens. Actuators, B*, 2001, **75**, 213–222.
12 M. Madou, J. Zoval, G. Jia, H. Kido, J. Kim and N. Kim, *Annu. Rev. Biomed. Eng.*, 2006, **8**, 601–628.
13 M. H. Moon, H.-J. Kim, S.-Y. Kwon, S.-J. Lee, Y.-S. Chang and H. Lim, *Anal. Chem.*, 2004, **76**, 3236–3243.
14 D. Huh, J. H. Bahng, Y. Ling, H. H. Wei, O. D. Kripfgans, J. B. Fowlkes, J. B. Grotberg and S. Takayama, *Anal. Chem.*, 2007, **79**, 1369–1376.
15 M. M. Wang, E. Tu, D. E. Raymond, J. M. Yang, H. Zhang, N. Hagen, B. Dees, E. M. Mercer, A. H. Forster, I. Kariv, P. J. Marchand and W. F. Butler, *Nat. Biotechnol.*, 2005, **23**, 83–87.
16 M. P. MacDonald, G. C. Spalding and K. Dholakia, *Nature*, 2003, **426**, 421–424.
17 A. Y. Fu, C. Spence, A. Scherer, F. H. Arnold and S. R. Quake, *Nat. Biotechnol.*, 1999, **17**, 1109–1111.
18 L. R. Huang, E. C. Cox, R. H. Austin and J. C. Sturm, *Science*, 2004, **304**, 987–990.
19 M. Yamada, M. Nakashima and M. Seki, *Anal. Chem.*, 2004, **76**, 5465–5471.
20 J. Takagi, M. Yamada, M. Yasuda and M. Seki, *Lab Chip*, 2005, **5**, 778–784.
21 S. Yang, A. Undar and J. D. Zahn, *Lab Chip*, 2006, **6**, 871–880.
22 M. Yamada and M. Seki, *Anal. Chem.*, 2006, **78**, 1357–1362.
23 M. Yamada and M. Seki, *Lab Chip*, 2005, **5**, 1233–1239.
24 S. Choi, S. Song, C. Choi and J.-K. Park, *Anal. Chem.*, 2009, **81**, 50–55.
25 S. Choi and J.-K. Park, *Lab Chip*, 2007, **7**, 890–897.
26 S. S. Kuntaegowdanahalli, A. A. S. Bhagat, G. Kumar and I. Papautsky, *Lab Chip*, 2009, **9**, 2973–2980.
27 J. Seo, M. H. Lean and A. Kole, *J. Chromatogr., A*, 2007, **1162**, 126–131.
28 D. Di Carlo, J. F. Edd, D. Irimia, R. G. Tompkins and M. Toner, *Anal. Chem.*, 2008, **80**, 2204–2211.
29 D. Di Carlo, *Lab Chip*, 2009, **9**, 3038–3046.
30 Z. Wu, B. Willing, J. Bjerketorp, J. K. Jansson and K. Hjort, *Lab Chip*, 2009, **9**, 1193–1199.
31 J.-S. Park, S.-H. Song and H.-I. Jung, *Lab Chip*, 2009, **9**, 939–948.
32 J.-S. Park and H.-I. Jung, *Anal. Chem.*, 2009, **81**, 8280–8288.
33 F. White, *Fluid Mechanics, WCB*, McGraw-Hill, New York, 1999.